Supporting Information

Atomic spin precession electro-optic modulation detection based on guided mode resonant lithium niobate metasurfaces

Jie Sun[1,2,3,4,5], Heng Yuan[6], Yuqing Yang[7], Zhibo Cui[1,2,3,4,5], Yuting Xu[1,2,3,4,5], Yan Xu[1,2,3,4,5], Yulan Fu[7] and Zhen Chai[1,2,3,4,5*]*

[1]Key Laboratory of Ultra-Weak Magnetic Field Measurement Technology Ministry of Education, School of Instrumentation and Optoelectronic Engineering, Beihang University, Beijing, 100191, China

[2]Institute of Large-scale Scientific Facility and Centre for Zero Magnetic Field Science, Beihang University, Beijing, 100191, China

[3]Hangzhou Extremely Weak Magnetic Field Major Science and Technology Infrastructure Research Institute, Hangzhou, 370051, China

[4]Beihang Hangzhou Innovation Institute, Hangzhou, 370052, China

[5]Hefei National Laboratory, Hefei, 230088, China

[6]School of Instrumentation and Optoelectronic Engineering, Beihang University, Beijing 100191, China

[7]Institute of Information Photonics Technology, School of Physics and Optoelectronic Engineering, Beijing University of Technology, Beijing, 100124, P.R. China.

Fig. S1. Imaging of the device.

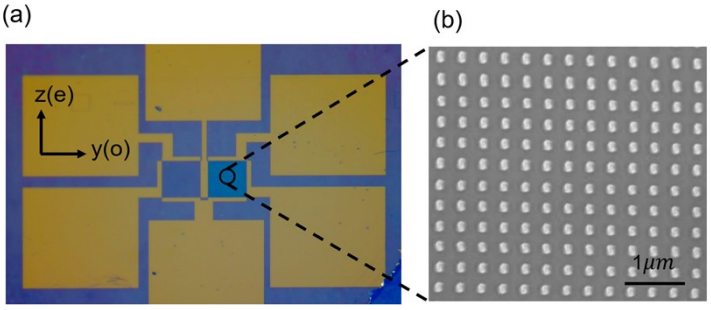

Figure S1. Imaging of the device. (a) The photograph of the fabricated modulator device. (b) The SEM images of the sample.

Fig. S2. Angular variations in simulated transmission spectrum.

The relationship between the incident angle and transmission spectrum was simulated, as shown in Figure S2. Clearly, when the incident angle deviates from the normal direction, the single resonance quickly turns into a double resonance, which is a characteristic phenomenon of GMR.

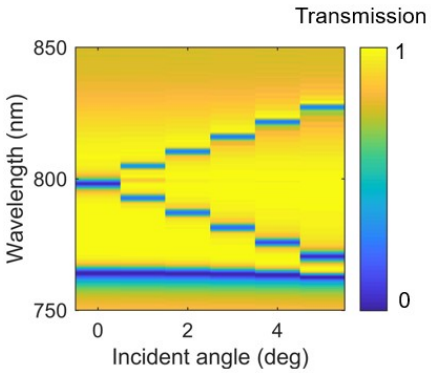

Figure S2. Angle variations in simulated transmission spectrum.

Fig. S3. Simulation and experimental results of the transmission spectra for two samples.

In addition to the set of parameters optimized in the text, we also calculate another set of parameters: D = 212 nm, H = 120 nm, P = 440 nm. In the second set of parameters, the diameter of the nanopillars is smaller than Sample 1 (D=270 nm), which may lead to increased fabrication errors. Simulations and tests were conducted on the transmission spectra of Sample 1 and Sample 2 with the incident light at an angle of 1°, fully confirming that when the direction of incident light deviates from the normal, a single resonance peak splits into double resonance peaks. The white arrows in the figure indicate the optical axis. From the test transmission spectra, it is observed that the lowest transmission rate of Sample 1 drops below 30%, while that of Sample 2 reaches 60%.

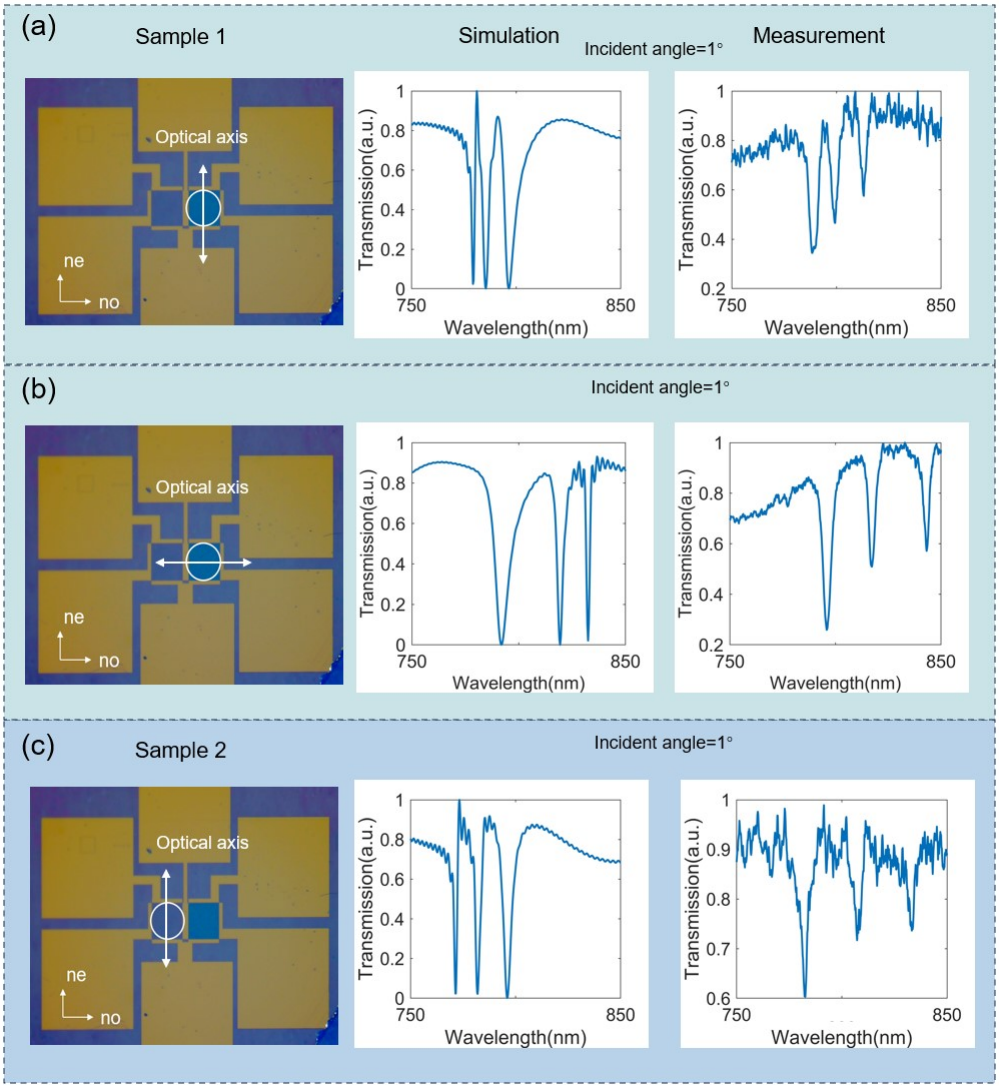

Fig. S3. Simulation and experimental results of the transmission spectra for two samples. (a), (b) Simulation and experimental transmission spectra of Sample 1 at an incident light angle of 1° under two polarization directions. (c) Simulation and experimental transmission spectra of Sample 2 with the incident light polarization parallel to the ne axis, at an incident angle of 1°.

S4. Pictures showing electro-optic characterization of the free-space GMR modulators

We built an electro-optical modulation performance characterization setup to evaluate the modulation performance of the samples under high-frequency driving voltages. Figure S4 presents camera pictures of the laboratory setup, a 500 μm collimator is used to produce linearly polarized incident light, which passes through a mirror and a linear polarizer. The light is then focused onto the plane of the sample. A distributed Bragg reflector (DBR) laser was chosen to generate free-space laser beam, and the center wavelength is around 795nm. The laser path is represented by the red arrows. Figure S4(b) shows an image captured with a 10× objective combined with a CMOS camera. The white circles mark the positions of the electrodes and the probe on the lithium niobate thin film of two samples, aligning with their extraordinary axes to ensure that the laser beam targets the appropriate sample locations. Figure S4(c) displays an image taken with a 12.5× objective combined with a camera, showing the needle in contact with the surface electrodes of the sample, ensuring that voltage can be applied to the sample.

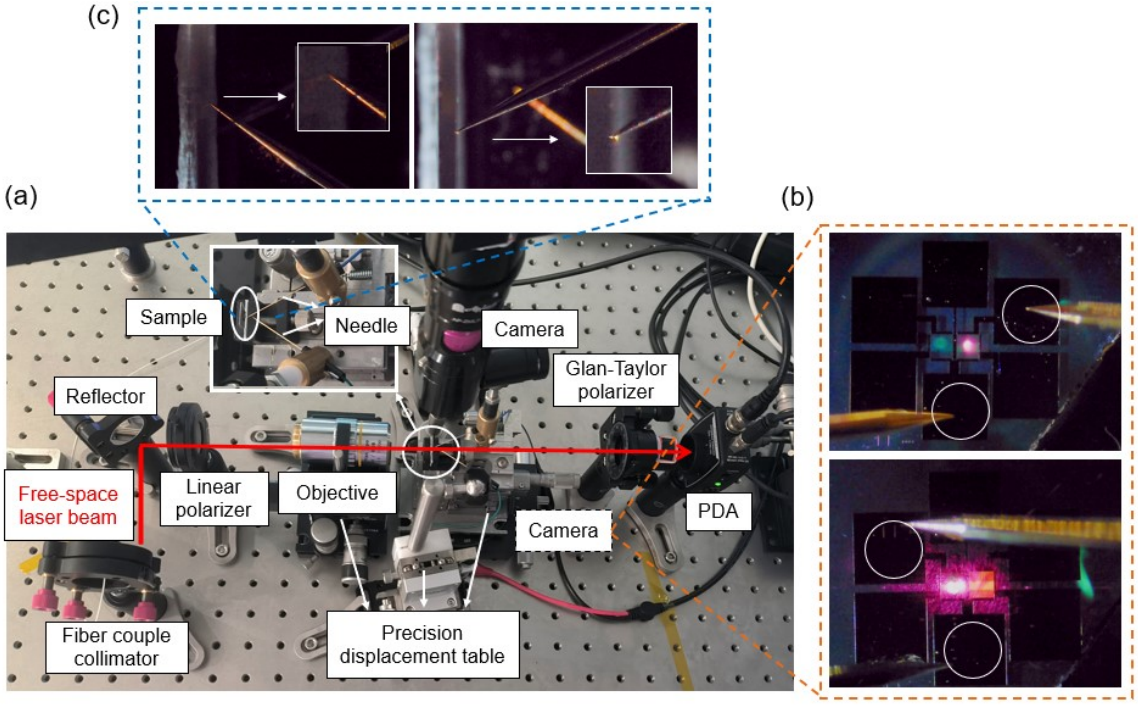

Figure S4. Pictures showing electro-optic characterization of the free-space GMR modulators. (a) Simplified setup sketch. PDA: Photodiode amplifier detector. (b) Photograph of different samples and corresponding electrode positions. (c) Photograph of the probe needle in contact with the sample.

S5. Frequency spectrum response of the Sample 2 at 50kHz and 100kHz.

The modulation performance of sample 2 was tested, and the frequency spectrum response at 50 kHz and 100 kHz was shown in Figure S5. The signal-to-noise ratio of the response signal is significantly lower than that of sample 1.

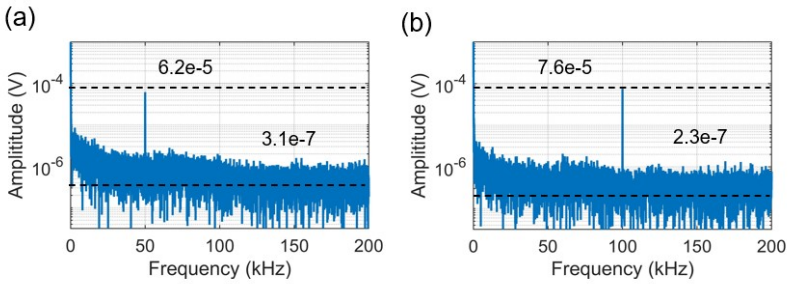

Figure S5. Frequency spectrum response of the sample 2. (a) Frequency spectrum response at 50 kHz. (b) Frequency spectrum response at 100 kHz.